Neuron
Article

Multiple Clusters of Release Sites Formed by Individual Thalamic Afferents onto Cortical Interneurons Ensure Reliable Transmission

Martha W. Bagnall,[1,2,4,*] Court Hull,[1,2] Eric A. Bushong,[3] Mark H. Ellisman,[3] and Massimo Scanziani[1,2,4,*]
[1]Center for Neural Circuits and Behavior
[2]Neurobiology Section, Division of Biology
[3]National Center for Microscopy and Imaging Research, Center for Research in Biological Systems, Department of Neurosciences
University of California, San Diego, La Jolla, CA 92093, USA
[4]Howard Hughes Medical Institute, La Jolla, CA 92093, USA
*Correspondence: mbagnall@northwestern.edu (M.W.B.), massimo@biomail.ucsd.edu (M.S.)
DOI 10.1016/j.neuron.2011.05.032

SUMMARY

Thalamic afferents supply the cortex with sensory information by contacting both excitatory neurons and inhibitory interneurons. Interestingly, thalamic contacts with interneurons constitute such a powerful synapse that even one afferent can fire interneurons, thereby driving feedforward inhibition. However, the spatial representation of this potent synapse on interneuron dendrites is poorly understood. Using Ca imaging and electron microscopy we show that an individual thalamic afferent forms multiple contacts with the interneuronal proximal dendritic arbor, preferentially near branch points. More contacts are correlated with larger amplitude synaptic responses. Each contact, consisting of a single bouton, can release up to seven vesicles simultaneously, resulting in graded and reliable Ca transients. Computational modeling indicates that the release of multiple vesicles at each contact minimally reduces the efficiency of the thalamic afferent in exciting the interneuron. This strategy preserves the spatial representation of thalamocortical inputs across the dendritic arbor over a wide range of release conditions.

INTRODUCTION

The activity of even a single thalamic axon can generate robust, widespread inhibition in somatosensory cortex (Swadlow and Gusev, 2000, 2002). This is not because thalamic afferents are inhibitory—they release the excitatory transmitter glutamate (Kharazia and Weinberg, 1994)—but because they can efficiently fire cortical inhibitory neurons through one of the cortex's most powerful synapses (Cruikshank et al., 2007; Gabernet et al., 2005; Hull et al., 2009; Porter et al., 2001; Swadlow and Gusev, 2000, 2002). These GABAergic interneurons in turn synapse onto local excitatory neurons, creating a robust feedforward inhibitory circuit (Gabernet et al., 2005; Inoue and Imoto, 2006; Sun et al., 2006) that may serve to tune the postsynaptic response, ensure temporal precision of spiking, widen dynamic range, and dampen intracortical excitation (Bruno and Simons, 2002; Gabernet et al., 2005; Pinto et al., 2003; Pouille et al., 2009; Pouille and Scanziani, 2001; Wehr and Zador, 2003; Wilent and Contreras, 2005).

Powerful synaptic connections are usually composed of many synaptic contacts distributed over the membrane of the postsynaptic neuron. The spatial distribution of these contacts can have major consequences on the excitation of the postsynaptic cell (Euler et al., 2002; Fried et al., 2002; Gouwens and Wilson, 2009; Losonczy et al., 2008; Poirazi and Mel, 2001; Segev and London, 2000; Williams and Stuart, 2003). Individual thalamic fibers excite cortical inhibitory neurons through ~15 synaptic release sites that release glutamate with high probability, yielding unitary excitatory conductances as large as 10 nS (average, 3 nS) (Cruikshank et al., 2007; Gabernet et al., 2005; Hull et al., 2009); however, little is known about the spatial configuration of these release sites on the dendrites of cortical neurons.

One can envision two opposite spatial configurations, each with profoundly different consequences on the excitation of the postsynaptic target. Release sites are (1) concentrated in one location (Figure 1A) or (2) distributed across the dendritic arbor (Figure 1B). In the first configuration, (e.g., the cerebellar mossy fiber to granule cell synapse), transmission is locally reliable and graded with respect to release probability. However, the contribution of each release site to postsynaptic depolarization is reduced due to the local decrease in driving force and increase in dendritic conductance. In the second configuration (e.g., the cortical layer 4 to 2/3 synapse), transmission is locally all-or-none. However, because release sites are electrotonically distant from each other, this configuration maximizes the contribution of individual vesicles of transmitter to postsynaptic depolarization.

We took advantage of Ca-permeable (GluA2-lacking AMPA and NMDA receptor-mediated) signaling at the thalamocortical synapse (Hull et al., 2009) to visualize the anatomical map of the unitary connection with Ca-sensitive dye imaging, as well as electron-microscopic analysis. We demonstrate that each

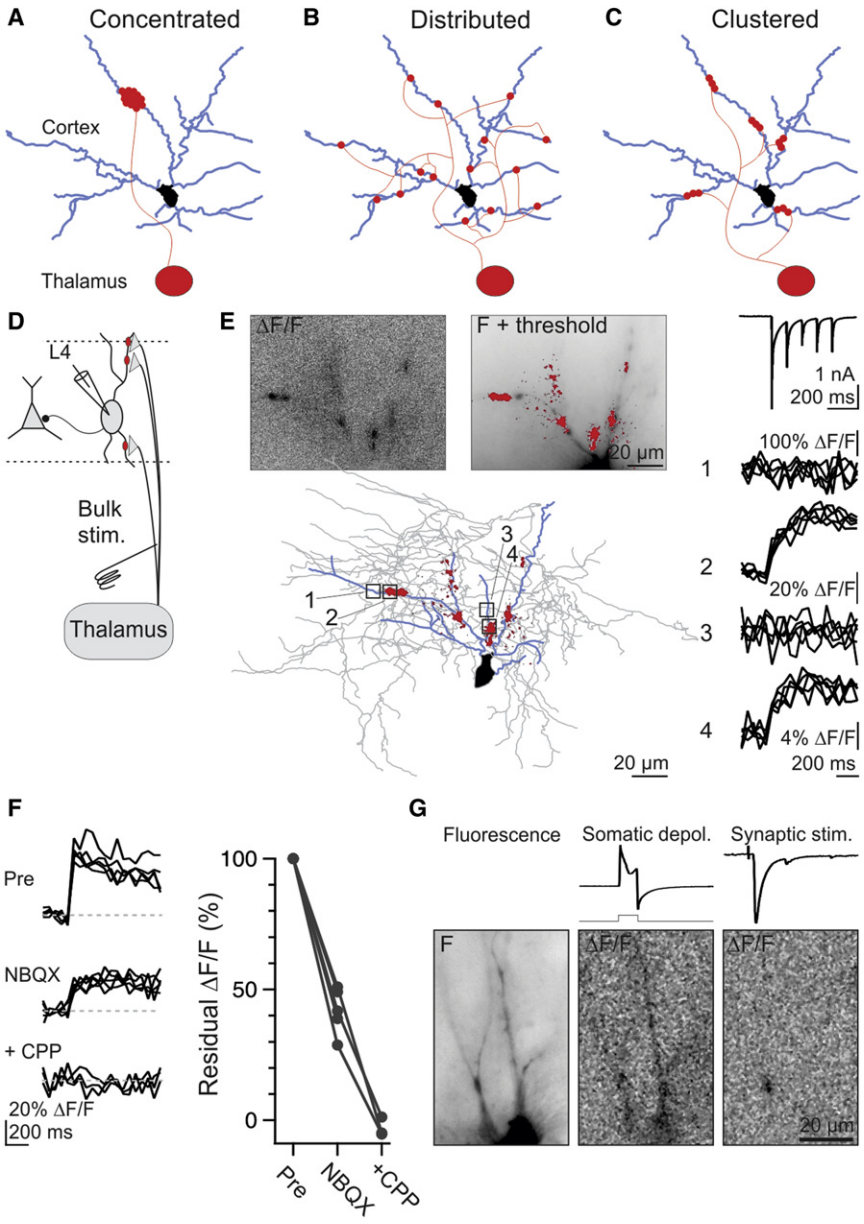

Figure 1. Stimulating Thalamic Axons Generates Ca Hotspots through Glutamate Receptor Activation

(A–C) Configurations by which an individual thalamic axon may contact a cortical interneuron; each dot is a release site: (A), concentrated, (B), distributed, and (C) clustered.

(D) Schematic of simultaneous physiological recording and Ca imaging from Layer IV interneurons during bulk stimulation of thalamic afferents.

(E) Top left: ΔF/F in response to bulk stimulation of thalamic afferents (average of five trials). Top right: thresholded ΔF/F (red) superimposed on fluorescence image of the recorded interneuron. Bottom: thresholded ΔF/F and reconstructed interneuron (blue, dendrites; gray, axon). Right traces, top: synaptic current evoked by thalamic afferent stimulation (5 stimuli at 10 Hz; average of 5 sweeps) recorded in voltage clamp at −65 mV while imaging the interneuron on the left. Traces 1–4: ΔF/F for four regions of interest (boxed areas on reconstruction).

(F) Left: elimination of a Ca transient resulting from a single stimulus by sequential application of NBQX and CPP. Right: summary data for similar experiments (NBQX, n = 5; +CPP, n = 3). See also Figure S1.

(G) Left: fluorescence image of recorded interneuron. Middle: ΔF/F in response to somatic depolarization (from −60 to +20 mV for 5 ms, repeated 3 times at 5 Hz); top traces: current and square voltage step). Right: ΔF/F in response to thalamic afferent stimulation (top trace: simultaneously recorded EPSC, amplitude 411 pA).

thalamic axon synapses on a given cortical interneuron through a third, intermediate, configuration (Figure 1C): multiple contacts distributed across the dendritic arbor of a cortical interneuron, each comprising several release sites. We further show that this spatial configuration provides for reliable, graded Ca transients at each contact, with minimal loss to inefficiency. As a result, sensory information entering the cortex maintains a stable spatial representation across the dendrites of the target cells, spike after spike.

RESULTS

To visualize the subcellular distribution of thalamocortical inputs to Layer IV inhibitory interneurons in the somatosensory barrel cortex, we took advantage of the fact that these synaptic currents are mediated by Ca-permeable AMPA and NMDA receptors (Hull et al., 2009), and thus should generate a measurable Ca transient in the postsynaptic compartment (Goldberg et al., 2003b). We recorded from fast-spiking interneurons (see Experimental Procedures) with patch pipettes containing the fluorescent Ca indicator Oregon Green BAPTA-1 (150 μM) in a slice preparation that preserves much of the thalamocortical fiber bundle (Agmon and Connors, 1991; Porter et al., 2001), allowing a stimulation electrode to be placed in this pathway slightly ventral to the fimbria. We simultaneously imaged the dendritic arbor of the recorded neuron (Figure 1D) and recorded the electrophysiological response in voltage clamp to stimulation of thalamic afferents.

We used three stimulation protocols: (1) bulk stimulation, in which multiple thalamic afferents are recruited; (2) threshold single fiber stimulation, in which a single afferent impinging on the recorded neuron or imaged dendrite is stimulated just at threshold, leading to fluctuation between recruitment successes and failures; and (3) single fiber stimulation, in which a single fiber impinging on the recorded neuron or imaged dendrite is

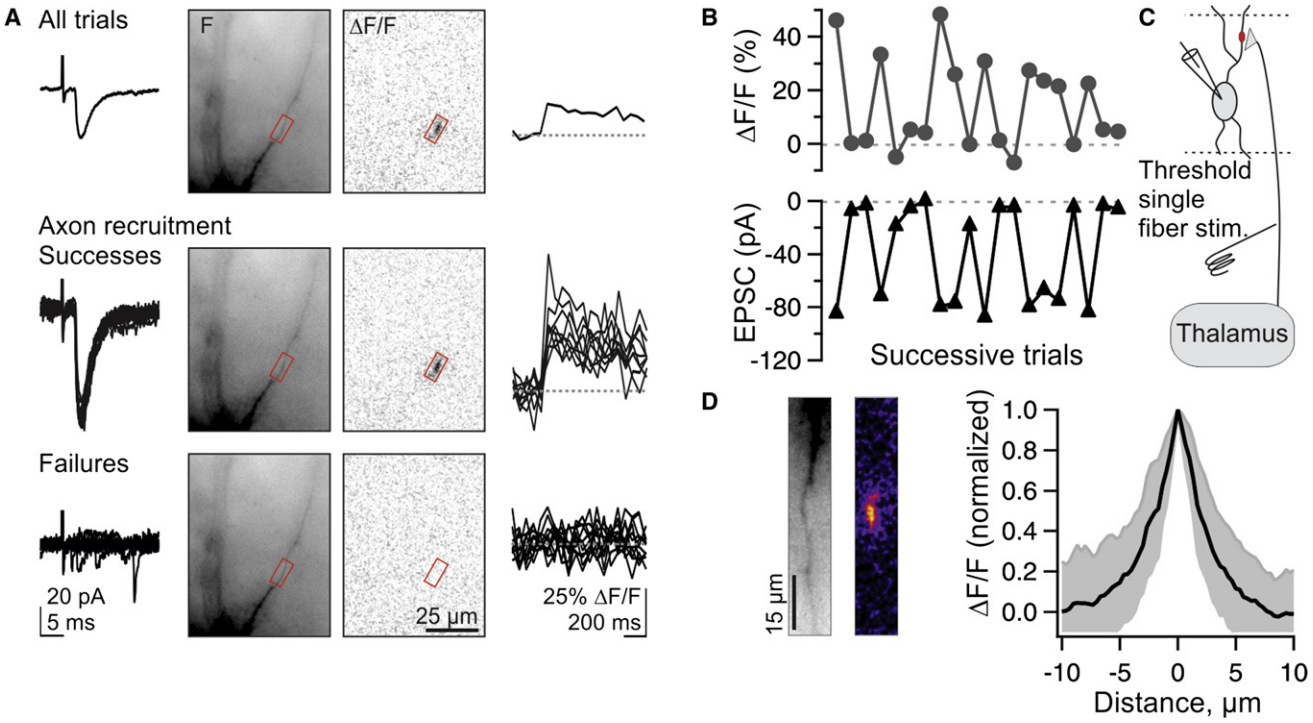

Figure 2. Activity of Individual Thalamic Axons Evokes Spatially Restricted Dendritic Ca Hotspots

(A) Threshold single fiber stimulation. Top row (from left to right): average uEPSC of 20 successive trials, recorded in voltage clamp. In this and subsequent figures, interneurons were clamped at −60 to −70 mV. Fluorescent image of recorded interneuron, ΔF/F, and time course of Ca transient recorded in the region of interest (red box). Middle and bottom: same as top but separated by individual successes (middle, 9 traces) and failures of axonal recruitment (bottom, 11 traces).

(B) Cofluctuation of successes and failures for Ca transients (top) and EPSCs (bottom) across successive trials of the experiment shown in (A).

(C) Schematic of the experiment: Ca transients represent the activity of individual thalamic afferents.

(D) Left: fluorescent image of dendrite. Center: ΔF/F of Ca hotspot on the same dendrite, with warmer colors representing larger ΔF/F. Right: Summary data for 64 hotspots: mean ± 1 standard deviation. Note the steep fall off of ΔF/F as a function of distance along the dendrite.

recruited reliably, without failures, by the stimulation electrode (see Experimental Procedures).

Postsynaptic Ca Hotspots Evoked by Stimulation of Thalamic Afferents

Bulk stimulation of thalamic afferents elicited a pattern of Ca hotspots—localized, transient postsynaptic increases in Ca concentration—decorating the dendritic arbor of cortical interneurons (Figure 1E). Addition of the AMPA-R antagonist NBQX reduced hotspot intensity by 58% ± 5% (n = 5), while further addition of the NMDA-R antagonist R-CPP eliminated hotspots entirely (to −1% ± 1%, n = 3; Figure 1F). Similarly, application of R-CPP reduced hotspot intensity by 59% ± 4% (n = 5; see Figure S1 available online), suggesting that Ca-permeable AMPA-R and NMDA-R contribute about equally to the postsynaptic Ca signal under our recording conditions.

Do hotspots mark the location of a synaptic contact? In the absence of perfect voltage clamp, hotspots could in principle result from the activation of voltage-gated Ca channels (VGCCs) not necessarily colocalized with the synaptic contact. To test this possibility, we monitored the spatial distribution of Ca transients in response to depolarizing voltage steps (Goldberg et al., 2003b). The resulting Ca transient was spread throughout the dendritic arbor (Figure 1G), indicating that VGCCs are distributed broadly and therefore unlikely to produce hotspots at significant distance from the site of synaptic contact. Thus, thalamic stimulation generates a spatial pattern of Ca transients that corresponds to the location of glutamate receptor-mediated thalamic inputs.

To ascertain whether an individual hotspot corresponded to the input of a single thalamic fiber, we used a threshold single fiber stimulation paradigm. For this, the stimulus strength was reduced to a level that produced fluctuations between successful and unsuccessful recruitment of a single thalamic axon impinging onto the recorded neuron, resulting in fluctuations between successes and failures of unitary excitatory postsynaptic currents (uEPSCs; average amplitude, 316 ± 57 pA, n = 21; 10%–90% rise time, 1.0 ± 0.2 ms, n = 21; 90%–10% fall time, 6.8 ± 0.5 ms, n = 20; means ± SEM) (Beierlein et al., 2003; Cruikshank et al., 2007; Gabernet et al., 2005; Gibson et al., 1999; Inoue and Imoto, 2006). EPSC latency (to 10% amplitude: 3.1 ± 0.11 ms, n = 21) and jitter (standard deviation [SD] of latency at 90% amplitude: 98 ± 60 μs, n = 17, mean ± SD) were both consistent with a monosynaptic origin. Even in response to stimulation of a single thalamic afferent, Ca hotspots could be detected on interneuron dendrites (Figure 2A). Importantly, Ca transients at the hotspot cofluctuated on a sweep by sweep basis with success and failure of the simultaneously

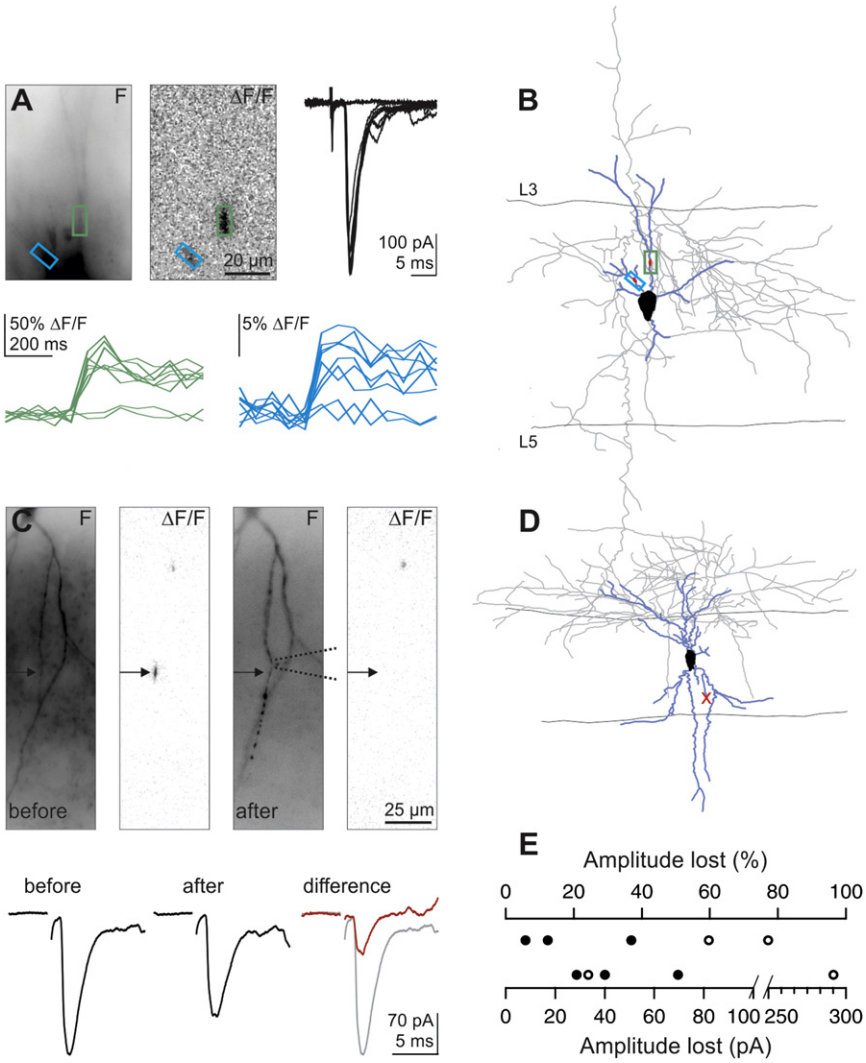

Figure 3. Individual Thalamic Axons Can Evoke Multiple Ca Hotspots

(A) Threshold single fiber stimulation. Top: fluorescence image of recorded interneuron (left), ΔF/F image (average of seven trials; center) and synaptic currents (seven successes and two failures; right). Bottom: successes and failures of Ca transients recorded in the color coded regions of interest illustrated above. Successes and failures of the two Ca transients cofluctuate with the successes and failures of the uEPSC.

(B) Reconstructed interneuron (blue, dendrites; gray, axon) from experiment in (A) with color coded regions of interest.

(C) Single fiber stimulation. Top: fluorescence image of recorded interneuron (left), ΔF/F image (average of six trials; second image), and fluorescence image (third image) and ΔF/F (right image, average of seven trials) after aspiration of dendrite (the dotted lines symbolize the position of the aspiration pipette). Bottom: average synaptic response before (left, average of six trials) and after (right; average of seven trials) aspiration of dendrite. Right: the difference between the synaptic response before and after dendritic aspiration (red trace) is superimposed on the average trace before aspiration (gray trace).

(D) Reconstructed interneuron (blue, dendrites; gray, axon) from experiment in (C). The red X marks the aspirated dendrite.

(E) Summary of five similar experiments. Closed circles represent experiments in which the dendrite was severed by aspiration; open symbols indicate those in which the dendrite was severely bent and the Ca hotspot disappeared.

recorded uEPSC, confirming that they resulted from the fluctuating threshold recruitment of a single thalamic afferent (Figures 2A and 2B). The spatial extent of hotspots evoked in response to the activity of a single thalamic afferent was restricted to a few μm along the longitudinal axis of the dendrite (length at half-maximum, 3.6 μm; n = 64; Figure 2D), which is likely an overestimate of the actual Ca domain due to the mobility of the Ca indicator (Goldberg et al., 2003a). Thus, hotspots correspond to the input of individual thalamic fibers (Figure 2C) and allow us to visually identify the subcellular location of contacts between a single thalamic axon and the interneuron dendrite.

Several Hotspots per Thalamic Axon

Does each thalamic fiber generate one or many hotspots? In response to threshold single fiber stimulation we were frequently able to detect two or more Ca hotspots whose occurrence cofluctuated with successes and failures of the uEPSC (see Figures 3A and 3B for examples; also see further statistics in Figure 8 from eight similar experiments). Thus, individual thalamic axons may contact the dendrites of interneurons through multiple hotspots, excluding the concentrated configuration of release sites illustrated in Figure 1A.

How many hotspots are generated by a single thalamic fiber? Because the number of detected hotspots per thalamic afferent is necessarily an underestimate due to limitations in visualizing the entire extent of the dendritic arbor, we used two independent approaches: (1) we determined the fractional contribution of each individual hotspot to the uEPSC by cutting the dendrite on which it was located, and (2) we estimated the number of release sites per hotspot and compared it to the total number of release sites per thalamic afferent (see below).

After a Ca hotspot was identified, the dendrite was aspirated with a patch pipette just proximal to the hotspot locus (Figure 3C). In three neurons the ablation was further confirmed by post hoc comparison of the biocytin fill of the dendrites with the live fluorescent dendritic image before the cut (Figure 3D). This led to a median reduction of the uEPSC of 37% (range, 6%–70%, 29-292 pA; n = 5; Figure 3E). The fact that cutting a hotspot-bearing dendrite did not abolish the uEPSC confirms our finding that individual thalamic afferents contact cortical interneurons through multiple loci and further indicates that these contacts must primarily occur onto distinct dendrites.

In addition, these data provide a lower bound estimate (because multiple contacts from one thalamic axon may be located on the same cut dendrite) of ~3 hotspots per thalamic afferent.

Several Release Sites per Hotspot

How many release sites compose a single hotspot? To address this question, we compared the release probability (P_r) of transmitter with the likelihood that afferent stimulation successfully generates a postsynaptic Ca transient in a given hotspot (P_{Ca}) during single-fiber stimulation. If each hotspot contains only one release site, as schematized in Figure 1B, we expect a linear relationship between synaptic P_r and P_{Ca}. In contrast, if N release sites are clustered in one hotspot, then P_{Ca} will exceed the synaptic P_r, with $P_{Ca} = 1 - (1 - P_r)^N$. We assessed the baseline P_r using variance mean analysis of a binomial model of release (Silver, 2003). Thalamocortical EPSCs were recorded in 3–5 different levels of Ca and Mg to vary P_r, in the presence of 1 mM kynurenate to minimize receptor saturation (Figure 4A) (Foster and Regehr, 2004). The resulting parabolic fit to the plot of EPSC variance versus mean amplitude at each Ca/Mg concentration (Figure 4B) was used to derive N and Q. P_r calculated for the 4 mM Ca, 0.5 mM Mg solution used in imaging experiments was 0.80 ± 0.06, whereas Q was 15.3 ± 3 pA (in the absence of kynurenate; n = 4), consistent with previous observations (Hull et al., 2009).

This high P_r makes it difficult to estimate the N at each hotspot locus over a small number of trials, due to the correspondingly low failure rate of postsynaptic Ca transients. Therefore, we reduced P_r pharmacologically with the $GABA_B$ receptor agonist baclofen (1–50 μM) and/or the adenosine A1 receptor agonist CPA (1–50 μM) (Fontanez and Porter, 2006). The resulting fractional reduction in EPSC amplitude, multiplied by the estimated initial P_r of 0.80, served as a measure of the reduced absolute P_r. We then monitored Ca transients across repeated trials to define P_{Ca}.

When P_r was moderately reduced to ~0.5, P_{Ca} still hovered close to 100% (Figure 4C), indicating that more than one release site contributes to a single hotspot and excluding the configuration illustrated in Figure 1B. When P_r was reduced to 0.2–0.4, the substantial number of failures of the Ca transient (Figure 4D) revealed that N ranged from 1.5 to 7, with an average of 3.4 ± 0.4 release sites per hotspot (n = 18 hotspots; excluding 3 hotspots where $P_{Ca} = 1$; Figure 4E). Thus, consistent with the clustered configuration illustrated in Figure 1C, multiple vesicles are released at each hotspot, a finding that is relatively insensitive to the precise value of the estimated P_r (see Discussion). Given the average of 15–20 release sites per thalamic axon (average 315 pA uEPSC divided by average Q of 15 pA) (Hull et al., 2009), these data suggest that each thalamic afferent forms, on average, 4–6 such clusters (schematic, Figure 1C).

Graded, Reliable Ca Transients Maintains a Stable Thalamic Representation

What are the functional consequences for postsynaptic Ca transients of clustering multiple release sites together? The clustering of release sites suggests that Ca transients at each hotspot should be reliable, spike after spike, and graded, i.e., variable in proportion to P_r. We compared the response of Ca hotspots to single versus repeated stimulation of the thalamocortical pathway. Despite ~50% depression of P_r by the second of two consecutive stimuli delivered at 1 Hz (as evaluated by the depression of the simultaneously recorded EPSC amplitude; Figure 5A), the second Ca transient at hotspots was very reliable (6% ± 3% failures, n = 7), The same was true for the last Ca transients of a train of 10 stimuli delivered at 1 Hz (10th stimulus, 16% ± 5% failures, n = 8 hotspots from 7 neurons, different set than paired-pulse). Similar results were obtained in adult (>P39) animals (17% ± 2% failure rate, n = 4). This indicates that Ca transients at hotspots are reliable despite large variations in P_r.

Decreasing P_r through repetitive stimulation reduced the amplitude of individual Ca transients (remaining amplitude of successful Ca transients, 51% ± 3%, n = 11; Figure 5D) as did reducing P_r pharmacologically (baclofen and/or CPA; see above; 44% ± 4%; n = 19, Figure 5D). Importantly, the amplitude of the average of successful Ca transients was proportional to the decrease in P_r (Figure 5D; average remaining P_r 53% ± 2% for paired-pulse, 51% ± 3% for pharmacological reduction), suggesting that the local Ca concentration at hotspots varies in a graded manner with P_r.

Are Ca hotspots composed of several spatially isolated Ca microdomains, each generated by one release site, or do all release sites contribute to a common postsynaptic Ca pool? If release sites share postsynaptic glutamate receptors, they by definition would contribute to a common postsynaptic Ca pool. The low-affinity competitive glutamate receptor antagonist γ-DGG can be used to identify changes in cleft glutamate concentration due to changes in the number of active release sites with shared access to a pool of receptors (Tong and Jahr, 1994; Wadiche and Jahr, 2001). We used paired pulse stimulation of thalamic afferent to compare the antagonism of γ-DGG on EPSCs generated by high (first pulse) versus low (second pulse) P_r.

On average, γ-DGG (1 mM) reduced the first EPSC by 38% ± 3%, and the second EPSC by 56% ± 3% (n = 12; $p < 0.0001$; seven single thalamic fiber stimulation and five bulk stimulation) (Figures 6A and 6B), indicating changes in cleft glutamate concentration with changes in P_r. In contrast, application of the high-affinity antagonist NBQX at low concentration (100 nM) yielded similar amplitude reductions of both the first and second EPSC (Figure 6B). These results indicate that glutamate originating from distinct release sites accesses a common set of postsynaptic glutamate receptors. Thus, release sites contribute to a common postsynaptic Ca pool whose concentration varies with P_r. Finally, γ-DGG did not affect the decay time constant of the EPSC (2% ± 8% change of weighted decay; n = 9), consistent with glutamate pooling between closely spaced release sites (DiGregorio et al., 2002).

Multiple Release Sites at a Single Contact

The observed clustering of release sites might occur either through (1) separate boutons arising from a single axon converging, closely spaced, on one dendritic locus or (2) a single bouton capable of releasing multiple vesicles. To distinguish between these possibilities, we pursued electron microscopy to examine synaptic ultrastructure.

Pre-embedding immunostaining for the glutamate transporter VGluT2 was used to identify axonal boutons arising from

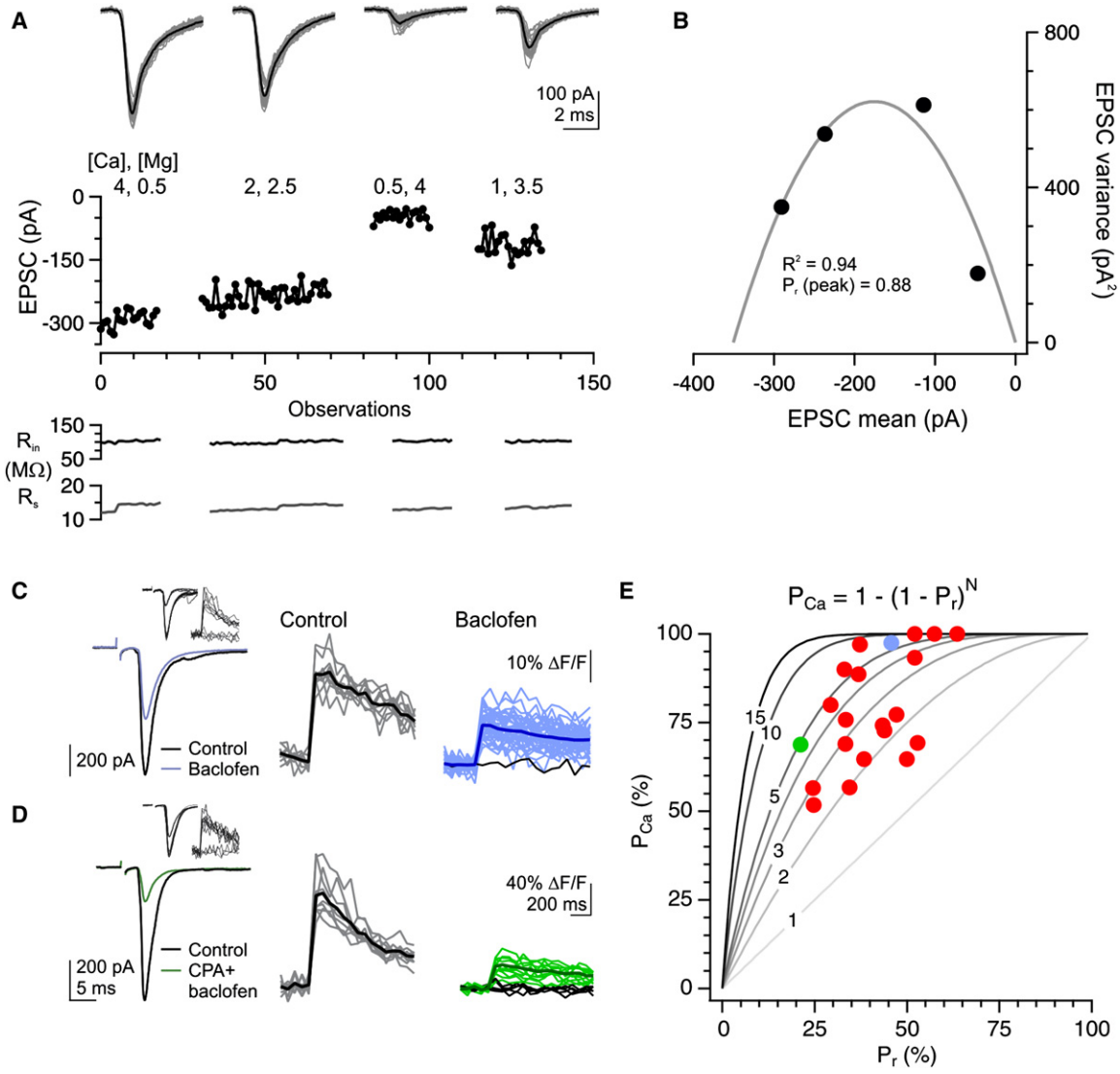

Figure 4. Three Release Sites, on Average, Compose a Single Hotspot

(A) EPSCs recorded in an interneuron during bulk stimulation of thalamic afferents under various concentrations of divalent ions and 1 mM kynurenate. In this example some bath solutions were washed in twice; sweeps are grouped together by condition (gray: individual sweeps, black: average).

(B) Fitting the EPSC variance and mean to a binomial model yields a P_r of 0.88 for this cell in the 4 mM Ca, 0.5 mM Mg condition.

(C) Application of the $GABA_B$ receptor agonist baclofen reduced the EPSC (left) by 43% but the Ca transient at the hotspot failed on only 1/39 trials (2.6%; right, black trace). Average of successful Ca transients is shown in black (control, center) or dark blue (baclofen, right). In this example, a lower-threshold thalamic axon is also recruited but does not contribute to the Ca hotspot (inset, EPSC and Ca transients during 13 sequential trials of threshold single-fiber stimulation).

(D) As in (B), for a second example neuron in which both baclofen and the A1 receptor agonist CPA were used to reduce the EPSC by 75%; Ca transient at the hotspot succeeded on 11/16 trials (69%). Inset, EPSC and Ca transient during threshold single-fiber stimulation.

(E) Data from 21 neurons (red dots) in which baclofen and/or the A1 agonist CPA (each 1–50 μM) were used to reduce P_r. Gray lines indicate the predicted relationship between Ca transient success rate (P_{Ca}) and P_r for the given number of release sites in a hotspot. The example neuron shown in (C) is colored blue; that in (D) is colored green. Excluding cells for which the Ca transients were successful on 100% of all trials (n = 3), the average N was 3.4 ± 0.4 release sites (SEM; n = 18).

thalamic sources (Fremeau et al., 2001; Hur and Zaborszky, 2005; Nahmani and Erisir, 2005), while parvalbumin expression identified postsynaptic L4 interneurons. Four axodendritic contacts were reconstructed from serial images spanning 10–15 ultrathin sections (~0.8–1.2 μm). In one instance, the nearest neighbor thalamic bouton was seen >350 nm distant (edge to edge); in the other instances, no other thalamic bouton was found within the entirety of the reconstruction nor in nearby scanning. Presynaptic terminals were of moderate size (0.14 ± 0.04 μm^3) and contained many clear, round vesicles as well as, in three of four cases, a mitochondrion (Figure 7A), consistent with previous reports (Kharazia and Weinberg, 1994; Staiger et al., 1996). Postsynaptically, the postsynaptic density (PSD) was unperforated and presented a synaptic surface area of

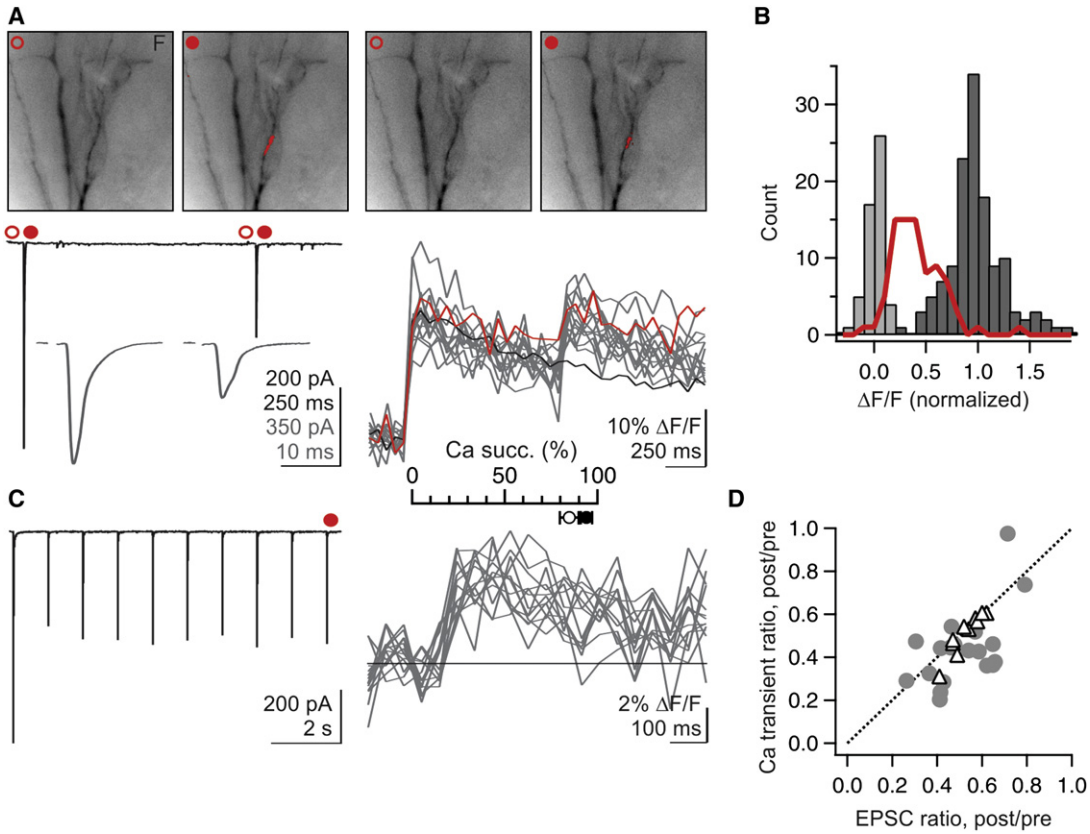

Figure 5. Clustered Release Sites Ensure Locally Reliable Transmission

(A) Single fiber stimulation. Top: each of two consecutive stimuli of thalamic afferents elicits a reliable hotspot, despite the ~50% depression of the second EPSC. Fluorescence images before and after the first (left) and second (right) stimulus, with overlaid thresholded ΔF/F. Images are averages of three frames from a single trial. Bottom: average EPSCs evoked by the two stimuli on two different time scales (left) and individual Ca transients in response to the two stimuli (14 superimposed traces). The example trial on top is shown in red. Black, the average Ca transient to a single stimulus (average of 14 traces).

(B) Ca transients at a hotspot are graded. Distribution of ΔF/F values for individual trials in response to two consecutive stimuli for seven experiments similar to (A). ΔF/F values are normalized by the average ΔF/F in response to the first stimulus. Dark gray: ΔF/F in response to first stimulus; red: ΔF/F in response to second stimulus; light gray: ΔF/F in response to "second" stimulus on interleaved 1-stimulus trials, as an indication of the noise. The Ca transient at each hotspot in response to the second stimulus is approximately half the Ca transient to the first stimulus.

(C) Single fiber stimulation. EPSC and Ca transient resulting from 10-stimulus trains in a different cell. The Ca transient to the 10th EPSC was successful in 13/13 trials. The average response during the same time period to interleaved 9-stimulus trials has been subtracted from the ΔF/F (black line indicates 0). Inset, summary of fraction of trials with successful Ca transients to the last stimulus for paired-pulse stimuli (filled circles, n = 7 cells) and 10-stimulus trains (open circles, n = 8).

(D) Triangles: the average ratio of the second versus first Ca transient elicited by two consecutive stimuli is plotted against the ratio of the second versus first EPSC evoked by the same two stimuli (n = 11). Circles: the average ratio of the Ca transient recorded after versus before baclofen and/or CPA application is plotted against the ratio of the EPSC recorded after versus before the same conditions (n = 21). Ca transient failures are excluded from the averages (in both conditions), to illustrate the graded nature of the Ca signal at each hotspot. See also Figure S2.

0.11 ± 0.02 μm^2. In contrast, the PSDs at thalamic inputs to spines of excitatory neurons, visible in the same samples, sometimes exhibited perforations (Figure 7B) (Kubota et al., 2007), demonstrating that the images were of sufficient resolution and clarity to distinguish perforated from unperforated PSDs. The data are thus consistent with each bouton being capable of multivesicular release to a single PSD rather than separate boutons converging on one dendritic locus.

Distribution of Ca Hotspots across the Dendritic Arbor

We determined the spatial distribution of Ca hotspots across the dendritic arbor of cortical interneurons by post hoc reconstruction of recorded neurons. The fluorescence image from live recordings was matched with the reconstructed morphology allowing the localization of 85 Ca hotspots from 53 neurons (e.g., Figure 3A) and the distribution of all hotspots aligned on the average dendrogram of all reconstructed neurons (Figure 8A). Hotspots were preferentially located on proximal dendrites (median distance to soma: 50 μm; 95% of all hotspots located within 115 μm of the soma; Figure 8B; 5th to 95th percentile, 15–115 μm). This sharp drop-off in hotspot distribution >100 μm from the soma was not due a failure to detect more distal hotspots since comparison of live fluorescence images of dendrites with biocytin-filled reconstructions shows that the

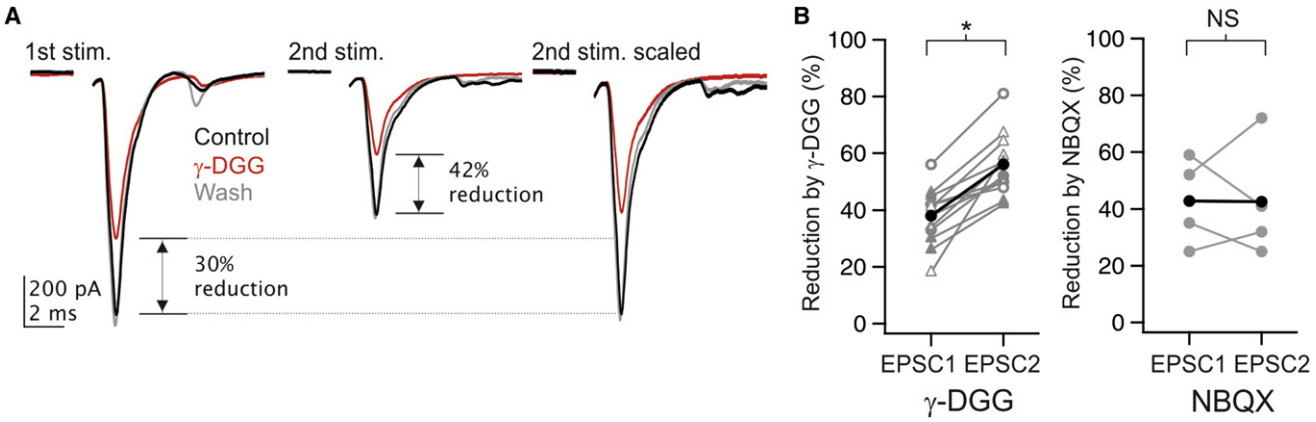

Figure 6. Diffusional Domains of Multiple Vesicles of Glutamate Overlap at a Common Pool of Postsynaptic Receptors

(A) Bath application of 1 mM γ-DGG during a paired-pulse stimulus reduced the first EPSC by 30% and the second EPSC by 42% in this example neuron. Right: the second EPSC scaled to match the peak of the first EPSC shows the relatively greater effect of γ-DGG, indicating a decrease in glutamate concentration. (B) Left: summary of data from 12 cells, recorded during single-fiber stimulation of thalamic afferents (open symbols) or bulk stimulation (closed symbols), showing a significantly larger effect of DGG on the second as compared to the first EPSC ($p < 0.0001$). Data collected at ~21°C are represented as circles, those at ~32°C as triangles. (Right: in contrast, low concentrations (100 nM) of the high-affinity antagonist NBQX did not have a differential effect on the first and second EPSCs.

first ~200 μm of dendrite were fully visible under fluorescence (Figure S3).

Hotspots were disproportionately found near dendritic branch points: 22.2% of all hotspots were located within 3 μm of a branch point, versus only 7.3% of the dendritic arbor (Figure 8C; N = 81 hotspots from 50 neurons; median distance from node, 10.4 μm versus random distribution, 25.7 μm; $p < 0.0001$, Mann-Whitney test; see Experimental Procedures).

There was no spatial relationship between the location of multiple hotspots arising from a single fiber (diamonds with same color): the likelihood that two hotspots from the same axon were found on the same dendrite as each other was 0.25, similar to chance (0.29 likelihood based on dendrite length for pairwise comparisons of hotspots arising from single axons; N = 18 hotspots from 8 thalamic axons). Furthermore, the correlation between the distance from the soma of two hotspots generated by the same axon ($r^2 = 0.33$) was not significantly different than the correlation between randomly chosen hotspot pairs within our population ($r^2 = 0.19$) ($p = 0.33$; see Experimental Procedures). These results indicate that thalamic inputs to interneurons are distributed onto proximal dendrites, preferentially near dendritic branch points.

Strong Synapses Form More Ca Hotspots

The amplitude of thalamic uEPSCs exhibits a >10-fold range, from ~1–10 nS (Cruikshank et al., 2007; Gabernet et al., 2005). Does a large-amplitude uEPSC derive from synaptic contacts located closer to the soma, from an increased potency of each contact, or from the formation of more contacts with the postsynaptic neuron? We found no correlation between uEPSC amplitude and hotspot distance from soma (Figure 8D, left; $R^2 = 0.04$, $p = 0.11$), ruling out the possibility that large-amplitude connections preferentially target the most proximal dendrites. Data from experiments in which a hotspot was removed by dendritic aspiration showed that the amplitude of the excitatory current generated by an individual hotspot did not correlate with the amplitude of the uEPSC ($R^2 = 0.25$, $p = 0.40$), suggesting that a large amplitude uEPSC does not rely on larger individual contacts than a small amplitude uEPSC. Furthermore, there was no correlation between the amplitude of uEPSCs and the magnitude of the Ca transient (Figure 8D, middle; $R^2 = 0.02$, $p = 0.41$), or the number of estimated release sites of individual hotspots (Figure S2; $R^2 = 0.004$, $p = 0.78$). These results thus suggest that large amplitude uEPSCs do not result from an increase in synaptic strength of individual hotspots. In contrast, there was a correlation between the amplitude of the uEPSC and the number of detected Ca hotspots that arose from that thalamic afferent (Figure 8D, right). Despite the fact that the number of detected hotspots is likely an underestimate of the actual number of hotspots generated by an individual thalamic afferent, the correlation between detected hotspot number and uEPSC amplitude suggests that large unitary connections are generated by a greater number of contacts.

Multivesicular Release Provides Reliability with Minimal Loss of Efficiency

Clustering release sites in one location reduces the contribution of individual vesicles of transmitter to membrane depolarization because of the local increase in conductance and reduction in driving force (Rall, 1970). To quantify the relative efficacy of synaptic transmission we used computational modeling to predict somatic depolarization with respect to the configuration of thalamic inputs (Figures 1A–1C). Reconstructions of three interneurons were imported into the NEURON modeling environment (Hines and Carnevale, 1997). Sixteen sites in the dendritic arbor of each neuron were selected as synaptic loci such that the overall distribution of these loci mimicked the distribution of hotspots in our data set (see Experimental Procedures) (Figure 9A). The amplitude of the simulated synaptic conductance at each site was adjusted to produce a 5 mV somatic

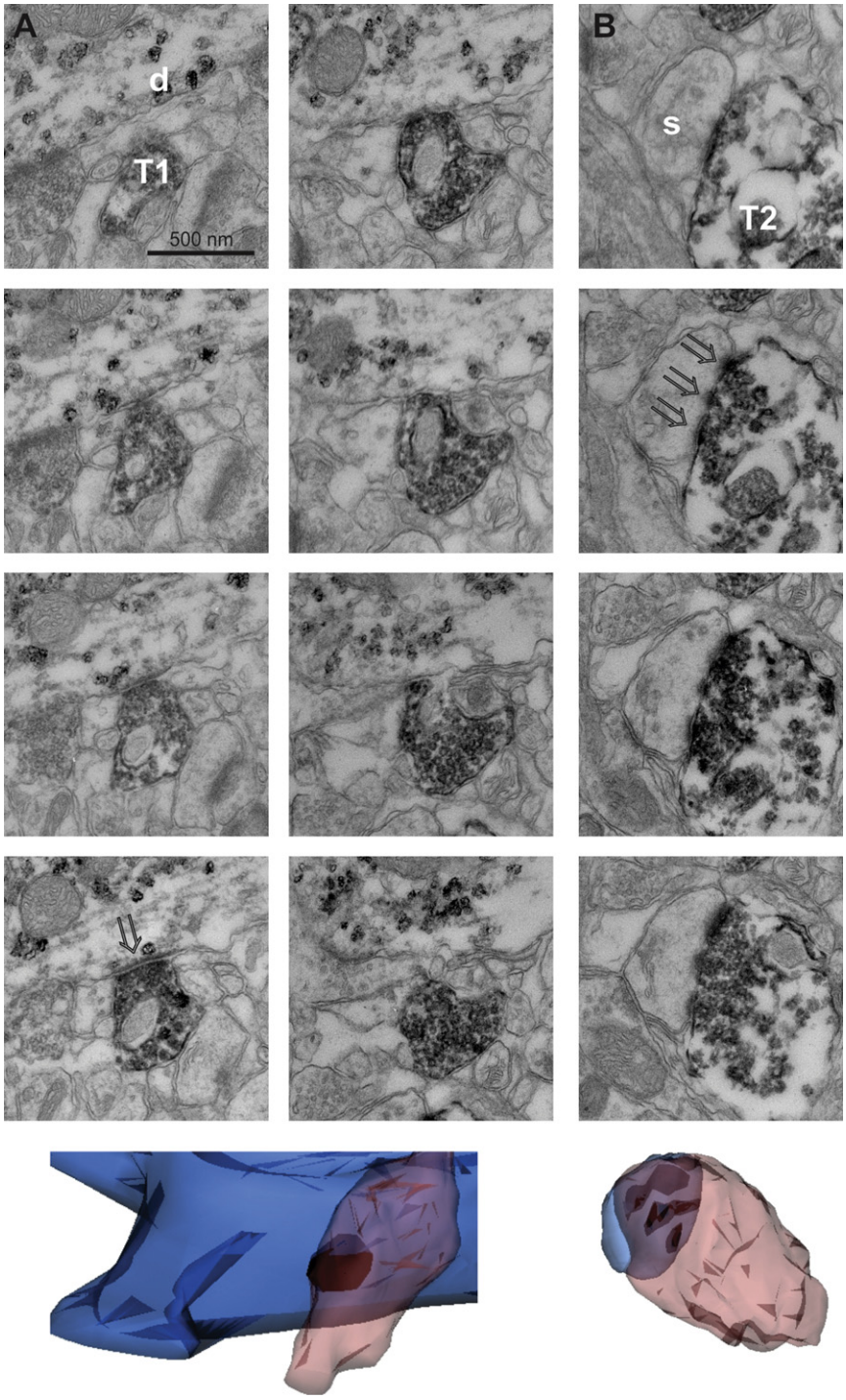

Figure 7. Ultrastructure of the Thalamic Input to an Interneuron

(A) Top: serial sections through the synaptic contact between a thalamic afferent (T1) and an interneuron dendrite (D), revealing a single bouton apposed to a single PSD (arrowhead). (Bottom) 3D reconstruction with the presynaptic thalamic bouton in peach, the postsynaptic dendrite in blue, and the PSD dark.

(B) Top: in contrast, afferent T2 synapses on an excitatory neuron spine (S) exhibiting a perforated PSD (arrowheads). Scale as in (A). Bottom: 3D reconstruction reveals three separate PSDs on this spine.

depolarization (Figure 9B). We then repeated this experiment using only 8, 4, 2, or 1 of the selected loci at a time, to imitate the effect of endowing each hotspot with clusters of 2, 4, 8, or 16 release sites, respectively. As expected, the total conductance required to achieve a 5 mV somatic depolarization increased with the increasing number of release sites at each locus, representing decreased efficiency of each release site as more sites are concentrated together. Noticeably, however, there was only a modest (~15%) decrease in efficiency as up to eight release sites were clustered together; a much greater inefficiency (~60%) occurred when all 16 modeled release sites were concentrated in one location (Figure 9C). These results thus indicate that as long as clusters do not contain more than eight release sites, the contribution of individual release sites to the overall membrane depolarization is not greatly impaired. Interestingly, the highest number of release sites per hotspot observed here was seven (see above and Figure 4E).

Active sodium and potassium conductances were not incorporated in this model because there are no reliable data on their distribution in cortical FS cells, and thus they would introduce significant free parameters. To evaluate whether these conductances would significantly affect dendritic summation of inputs, we used two-photon glutamate uncaging in recordings from L4 FS neurons. Glutamate was uncaged at two dendritic loci situated either on separate dendritic branches or right next to each other (<5 μm away) on one dendrite (Figure S5). In concordance with our modeling results, summation of both spatially separated and spatially clustered events was linear as long as the total event amplitude (recorded somatically) did not exceed ~5 mV (Figure S5B). These findings reinforce the conclusion of the model, that the local release of multiple quanta causes only modest inefficiencies of synaptic transmission.

DISCUSSION

The spatial distribution of inputs from an axon onto its target plays a key role in the way information is integrated by the

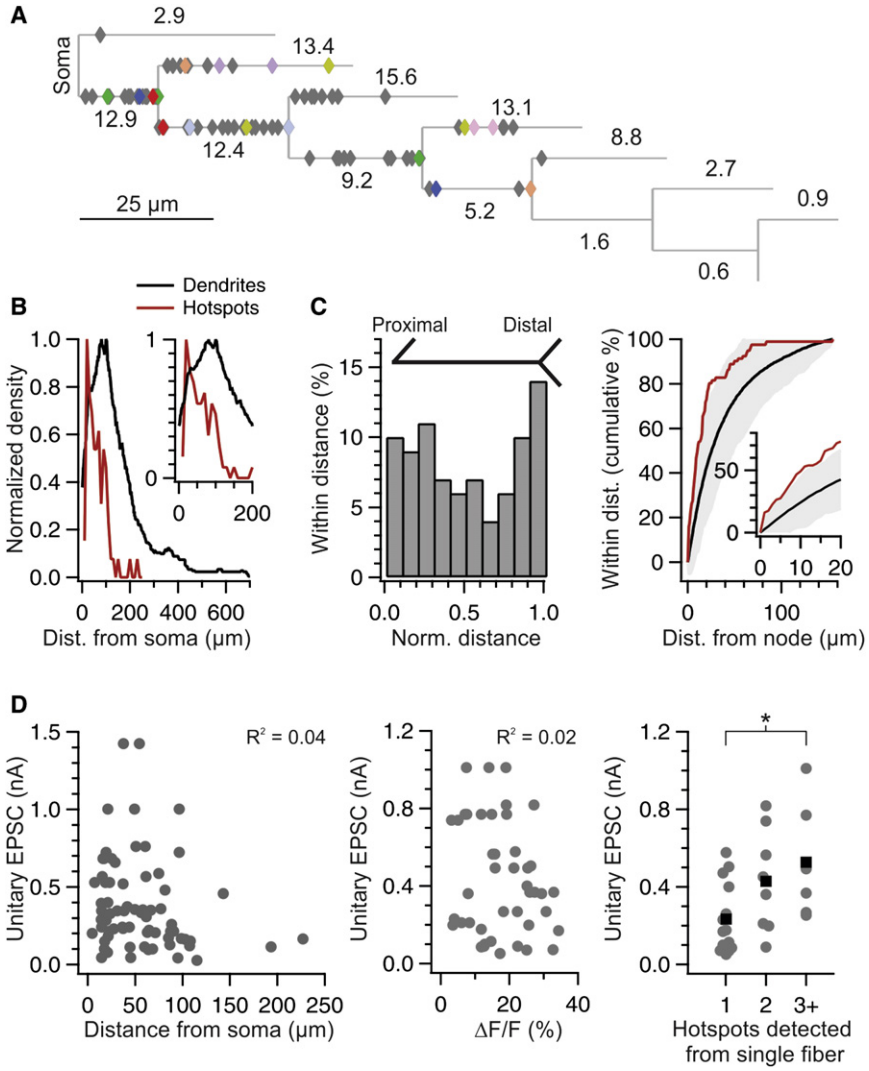

Figure 8. Distribution of Hotspots

(A) Average dendrogram of all reconstructed neurons (n = 53), with soma at left. Line length represents average straightened length of structures, e.g., tertiary branches that later bifurcate. Numbers indicate percentage of branches in each category (e.g., second-order terminal branches represent 13.4% of all branches). More distal branches, representing <1% of all branches, are not shown. Each diamond represents the location of a Ca hotspot (n = 85). Hotspots (diamonds) were placed on the dendrogram according to their structural location (e.g., halfway along a tertiary dendrite that later bifurcated), not according to their absolute distance from soma. Colored diamonds indicate pairs or triplets of hotspots generated by the activity of a single thalamic axon. The example neuron of Figure 3A is in red.

(B) Hotspots were detected more frequently in the proximal dendritic arbor. Normalized density of distribution of hotspots (red) and dendritic tree (hotspot-bearing dendrites only). Inset, magnified view of the first 200 µm.

(C) Hotspots occur preferentially close to dendritic branch points. Left: bimodal distribution of hotspots in a plot of normalized inter-node distance. Right: cumulative percentage of hotspots that fell within the given distance from a dendritic branch point, with inset for distances <20 µm. Black with gray shading indicates mean ± 2 × SD from repeated simulations of random hotspot distribution (see Experimental Procedures).

(D) Lack of correlation between uEPSC amplitude and hotspot proximity to soma (left; R^2 = 0.04, p = 0.11; n = 70) or with hotspot intensity (middle, R^2 = 0.02, p = 0.41; two large ΔF/F responses not shown). Large-amplitude uEPSCs are associated with higher numbers of Ca hotspots (right; means in black; *p = 0.03, Wilcoxon unpaired). See also Figure S3.

postsynaptic neuron. Although much is known about the physiological and pharmacological properties of the powerful synapse made by thalamic axons onto cortical inhibitory interneurons (Cruikshank et al., 2007; Gabernet et al., 2005; Gibson et al., 1999; Hull et al., 2009), the spatial organization of this input is unknown. Through Ca imaging we revealed that the contact sites (hotspots) of individual thalamic inputs are located on the proximal dendrites of L4 interneurons, preferentially near branch points. Each hotspot represents a single synaptic bouton capable of releasing up to seven vesicles simultaneously, and each thalamic axon forms a variable number of these boutons spread across the dendrites of individual cortical interneurons, depending on the strength of the input. This structure of many spatially separated synapses, each capable of multivesicular release, as schematically illustrated in Figure 1C, may have consequences for how sensory information is transmitted to cortical interneurons, because it promotes locally reliable and graded Ca transients while minimizing the inefficiencies of clustered release sites. Through such clusters, the spatial representation of thalamic sensory inputs onto the dendritic arbor is faithfully reproduced, spike after spike.

Distribution of Synaptic Contacts

Histological analyses revealed that hotspots were predominantly located on proximal dendrites, 95% occurring in the first 115 µm (Figure 8), consistent with ultrastructural studies (Ahmed et al., 1997; White et al., 1984; White and Rock, 1981). Together with structural data showing that ~15% of thalamic inputs to interneurons may be axosomatic (Ahmed et al., 1997; Staiger et al., 1996), and recent findings suggesting a similar proximal bias for thalamic inputs onto cortical excitatory neurons (Richardson et al., 2009), our data highlight one of the key parameters likely to contribute to the relative strength of thalamocortical inputs despite their numerical sparseness (Gil et al., 1999; Stratford et al., 1996). Synaptic contacts of a single axon were distributed on the dendrites independent of each other's location indicating the lack of dedicated dendritic domains (Figure 8) (Bollmann and Engert, 2009; Jia et al., 2010; Peron et al., 2009; Petersen et al.,

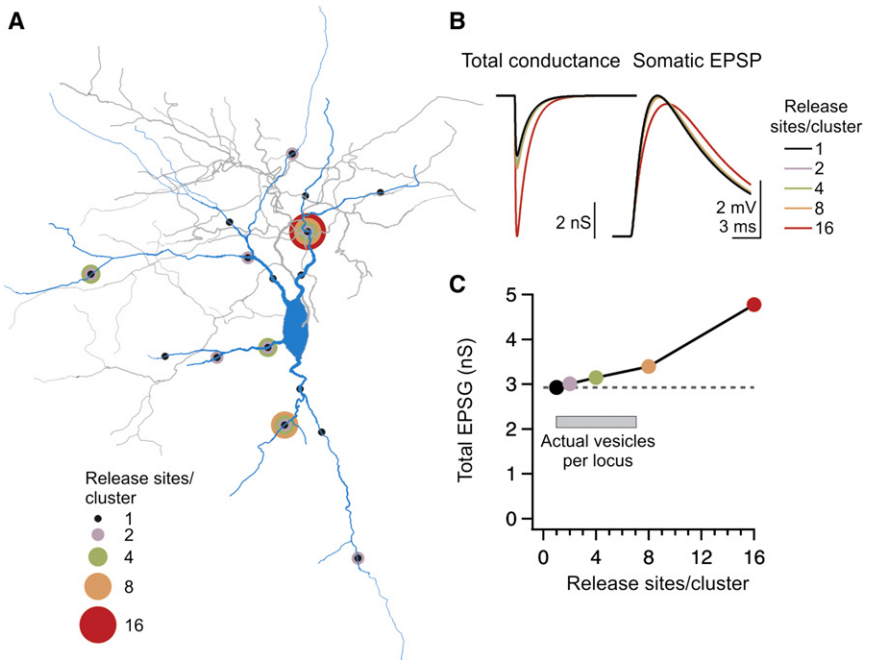

Figure 9. Clusters of Two to Six Release Sites Cause Only Modest Inefficiency of Transmission

(A) Reconstructed interneuron anatomy imported into the NEURON modeling environment. Circles represent the location of modeled clusters of release sites. The number of release sites per cluster is color coded. The arrangement shown is an example; 8–16 different arrangements of cluster locations were modeled in the 1, 2, 4, and 8 release sites/locus configurations.

(B) Left: the total conductance (sum of the 16 release sites) necessary to generate a somatic EPSP of 5 mV increases with cluster size. Right: the resulting average somatic EPSP in each condition.

(C) The median total conductance necessary to generate an 5 mV EPSP at the soma is plotted against cluster size for three neurons modeled as in (B). The required conductance for concentrations of 16 release sites is more than 50% larger than the conductance for clusters of 2–4 release sites. See also Figure S4.

2008). Furthermore, hotspots from the same axon were not located at similar distance from the soma as each other, suggesting the absence of an axon-specific uniform electrotonic distribution and consistent with the lack of correlation between the location of individual hotspots and the amplitude of the associated uEPSC (Figure 8A). Finally the lack of correlation between the number of release sites at a given hotspot and the amplitude of the associated uEPSC (Figure S2), suggest that larger uEPSCs do not result from an increased release sites per contact ratio. Rather, our data suggest that the uEPSC amplitude depends on the total number of synaptic contacts (Figure 8D).

Structure of Each Synaptic Contact

All but one of the hotspots examined exhibited evidence of multiple release sites (average 3.4 ± 0.4, n = 34 (Figures 4 and 5); a likely underestimate because we could not derive the number of release sites for the most reliable hotspots (n = 9 hotspots with no failures; Figures 4 and 5). We cannot exclude the possibility that contacts releasing only one vesicle were undersampled in our data set due to a selection bias toward more salient, and thus larger, more reliable, Ca transients. However, we were typically able to resolve events resulting from the release of a single vesicle (Figure 4D). Furthermore, recordings in the presence of the low-affinity antagonist γ-DGG, which are not biased by selection for imaging, revealed clear evidence for release of multiple vesicles (Figure 6). Therefore, single release sites are likely to represent only a small fraction of the total number of contacts.

The results of failure analysis (1–7 release sites per hotspot; Figures 4 and 5) are based on two assumptions: (1) that a P_r of 0.8 is homogeneous and (2) that the decrease in P_r is also homogeneous. However, if P_r were as low as 0.5, the calculated N would range from 1 to 13 with a mean of 6.0 ± 0.5 release sites/hotspot; if the P_r were as high as 0.95, N would range from 0.6 to 6 with a mean of 2.7 ± 0.2 release sites/hotspot (n = 31). The second assumption is supported by the relatively good match between the overall decrease in the P_r (as estimated by the decrease in EPSC amplitude) and the decrease in the amplitude of the Ca transient at an individual hotspot (Figure 5D and Figure S2).

The ultrastructure of this synapse has been studied previously (Benshalom and White, 1986; Kharazia and Weinberg, 1994; Staiger et al., 1996; White et al., 1984), but our data represent the first set of serial images, allowing for detailed analysis of the synaptic structure. The finding that each contact is composed of one bouton apposed to one PSD (Figure 7) is consistent with the γ-DGG experiments suggesting multi-vesicular release (DiGregorio et al., 2002; Tong and Jahr, 1994; Wadiche and Jahr, 2001; Kharazia and Weinberg, 1994; Staiger et al., 1996).

Functional Effects of Multivesicular Release

One consequence of releasing many vesicles from one bouton is that the occupancy of postsynaptic receptors will depend on the number of vesicles released and hence on P_r. Because the activation of these receptors contributes to the postsynaptic Ca transient, local Ca concentration will change progressively with changes in P_r, as can be observed with neuromodulators (Figure 4) (Chalifoux and Carter, 2010; Higley et al., 2009) or during repetitive presynaptic activity (Figure 5) (Hull et al., 2009). Thus, in response to each action potential, local Ca influx remains proportional to the global excitation of the cell. This mode of transmission contrasts with a spatial scattering of individual release sites, as observed between cortical pyramidal cells and interneurons (Koester and Johnston, 2005), or excitatory neurons (Silver et al., 2003), where local transmission is

all-or-none, and thus changes in P_r are reflected by changes in success rate over many action potentials.

Is release likely to be reliable in physiological conditions? Variance mean analysis provides an estimate of P_r of 0.31 (n = 3) at 1 Ca, 3.5 Mg, which represents a lower bound to release in comparison to physiological saline (~1.3 Ca, 1 Mg). At a P_r of 0.31, a bouton with an N of 3 would only produce failures in 33% of action potentials.

Computational and experimental studies of the consequences of clustering synapses have focused on the increased ability of a clustered connection to elicit supralinear responses via voltage-dependent dendritic conductances (Bollmann and Engert, 2009; Larkum and Nevian, 2008; Magee, 2000; McBride et al., 2008; Poirazi and Mel, 2001; Polsky et al., 2004; Segev and London, 2000). However, given the absence of dendritic spikes in hippocampal fast-spiking interneurons (Hu et al., 2010), the thalamic input to cortical interneurons is unlikely to drive regenerative dendritic activity. Instead, the release of multiple vesicles at one contact might cause sublinear summation due to the reduction in driving force caused by each additional quantum (Tamás et al., 2002). In fact, the thalamocortical input appears to be structured to limit nonlinearities by clustering no more than ~7 release sites in a single bouton (Figure 9 and Figure S5). Thus the configuration of 3–4 release sites per bouton allows for near-linear dendritic summation while causing only minor inefficiencies due to shunting.

In conclusion, the synaptic configuration reported here, that of several synaptic contacts, each containing a cluster of release sites, represents an intermediate configuration between the two extremes of anatomy: concentrated, like the mossy fiber synapses in the hippocampus and cerebellum (Salin et al., 1996; Saviane and Silver, 2006); and distributed like intracortical connections onto inhibitory neurons (Gulyás et al., 1993; Miles and Poncer, 1996; Geiger et al., 1997; Koester and Johnston, 2005).

Our findings build a picture in which thalamic inputs onto cortical inhibitory neurons target proximal dendrites with powerful synapses that elicit locally reliable, graded release. These results highlight the unique topological and functional strategy implemented by thalamic inputs to excite interneurons and thus reliably elicit cortical feedforward inhibition.

EXPERIMENTAL PROCEDURES

Electrophysiology

All experiments were conducted in accordance with UCSD animal protocols. Chemicals were from Sigma unless otherwise specified. Thalamocortical slices were prepared from juvenile (P14-25) or adult mice (P39-65; ICR White, Charles River) using cutting planes that preserve the ventroposteromedial thalamic nucleus and barrel cortex (see also Supplemental Experimental Procedures) (Agmon and Connors, 1991; Porter et al., 2001). Animals were anesthetized with Isoflurane; following decapitation, the brain was extracted and dissected in ice-cold sucrose solution (in mM: 83 NaCl, 2.5 KCl, 0.75 $CaCl_2$, 3.3 $MgSO_4$, 1.2 NaH_2PO_4, 26 $NaHCO_3$, 22 glucose, 73 sucrose).

Whole-cell recordings were carried out in a submerged chamber at room temperature (20–22°C) except for a subset of experiments in Figure 6 at 32°C–33°C using an Olympus BX51W1 microscope with a water-immersion 40× objective (NA 0.8). Slices were perfused with high Ca, low Mg artificial cerebrospinal fluid (in mM: 119 NaCl, 2.5 KCl, 1.3 NaH_2PO_4, 4 $CaCl_2$, 27 $NaHCO_3$, 0.5 $MgCl_2$, 20 glucose) to aid in visualizing hotspots. Pipette solution for all experiments except those involving glutamate uncaging contained (in mM): 140 K gluconate, 10 HEPES, 3 NaCl, 2 Na_2ATP, 0.3 NaGTP, 5 QX-314-Cl (Ascent Scientific), 0.15 Oregon Green 488 BAPTA-1 (OGB; Molecular Probes), and 0.3% biocytin.

Recordings were targeted to large, oblong somata in Layer 4 using DIC infrared video microscopy. Neurons were voltage clamped at −60 to −70 mV (uncorrected for junction potential, which was calculated as −14 mV [ClampFit]). Data were recorded with a Multiclamp 700B, digitized at 10 kHz with a Digidata 1322A, filtered at 2 kHz, and acquired in Clampfit 9 (Axon Instruments). Analysis was carried out in Igor Pro 5 (Wavemetrics) using custom-written routines.

Stimulation

Single fiber stimulation was performed and ascertained as described in Gabernet et al. (2005) and Hull et al. (2009). For "threshold single fiber stimulation" the stimulation intensity was set such that EPSC successes would randomly alternate with failures. For single fiber stimulation the threshold stimulation intensity was increased until EPSC failures were no longer evoked, yet the average amplitude of EPSC successes remained the same as during threshold stimulation (Figures 2D, 3C, 4C, 4D, and 5). At the beginning of every experiment, we used the "threshold single fiber stimulation" protocol to ensure that hotspot successes and failures cofluctuated with the simultaneously recorded EPSC, thus establishing the monosynaptic nature of the response to a single thalamic afferent (Figures 2A, 2B, and 3A). In some instances, the identified single thalamic fiber was not the lowest-threshold recruited fiber (Figures 4C and 4D, insets). During the rest of the experiment, the stimulation intensity was increased to reach the "single fiber stimulation" condition. (Gabernet et al., 2005; Hull et al., 2009).

Dendritic Aspiration

For the aspiration experiments in Figure 3, a second pipette was placed in close proximity to the dendrite of interest just proximal to the identified hotspot. Negative pressure was applied until the dendrite was drawn into the pipette. Aspiration was considered a success if the distal dendrite depolarized and began blebbing. Neurons were only included for analysis if the series resistance changed <15% in this process (average change, +5%) and the input resistance was stable (average change, −4%; n = 5).

Terminology

We refer to synapses as the sum of all contacts between an axon and the target neuron; contact or contact site as morphologically identifiable apposition between the pre-and postsynaptic membrane. Release site is a physiologically identifiable site of quantal release. A contact can have one or more release sites.

Imaging

Images were acquired with a cooled CCD camera (Till Imago-QE) in TillVision software. For fluorescence, the image was binned at 2 × 2; with a 40× objective, each pixel represented one-third micrometer. An LED with peak wavelength at 470 nm and total power of 210 mW (Thor Labs) provided illumination; each image was acquired over a 15 ms period at an overall rate of 15–20 Hz. Fluorescence intensity analysis was performed in TillVision and Microsoft Excel. A region of interest around a hotspot was selected, and two identically sized flanking background regions were averaged and subtracted from the fluorescence signal before carrying out ΔF/F analysis. To determine hotspot dimensions (Figure 2),the ΔF/F image along the longitudinal axis of the dendrite underwent a single pass of 3-pixel (1 μm) boxcar smoothing and traces were aligned at their peaks. We verified that the high-affinity Ca indicator OGB was not saturated by synaptic input (Figure S4).

Hotspot intensity is reported as the average of the first five image frames (300–340 ms) following stimulation. Successes of Ca hotspots on a sweep by sweep basis were defined as occurring when the ΔF/F of at least two of the five image frames following synaptic stimulation exceeded 2× the SD of the baseline period. During paired-pulse and 10-pulse analysis, successes of Ca hotspots were defined as occurring when the running integral of the five image frames following the second (or 10th) synaptic stimulation

exceeded the mean + 2× SD of the integral of interleaved single- (or 9-) stimulus trials, after all trials were scaled to the same baseline.

Histology

Slices containing biocytin-filled neurons were processed with diaminobenzidine (DAB) according to standard methods (see Supplemental Experimental Procedures). Neurons were imaged on a Zeiss Imager A1 microscope with a 63× objective (oil, NA 1.4). Cells were traced in Neurolucida 8 (MBF Bioscience). The live fluorescence image and the reconstructed outline were then compared to identify the precise location of the hotspot, and a marker was placed at the corresponding dendritic location. Analysis of morphology was then carried out in Neurolucida Explorer 4.

Most reconstructed neurons displayed axons and dendrites that arborized exclusively or predominantly in L4 (axons: 40/49 neurons; dendrites: 39/50). The remaining neurons extended processes to L2/3 and/or L5, and rarely beyond. All reconstructed neurons (50/50) were aspiny. QX-314 in the recording solution precluded characterization based on firing properties. Two classes of interneurons receive thalamic inputs (fast spiking [FS] parvalbumin expressing cells, and low threshold spiking somatostatin expression neurons) (Beierlein et al., 2003; Tan et al., 2008); only FS cells show the large-amplitude (uEPSC 315 ± 57 pA) and depressing thalamic input of the neurons included in this study (Beierlein et al., 2003). Furthermore, the input resistance (mean ± SD, 161 ± 51 MΩ, n = 52), membrane time constant (11.9 ± 3.8 ms, n = 50), EPSC kinetics (see Results), appearance under DIC IR video-microscopy and reconstructed morphology of the neurons included in this study is consistent with Layer 4 FS cells characterized in a separate data set in which QX-314 was not included in the intracellular solution (n = 49/52 had action potentials with half-widths under 1 ms [mean ± SD, 0.67 ± 0.13 ms] and spike rates in excess of 100 spikes/s) as well as previously described in this lab (Gabernet et al., 2005; Hull et al., 2009).

Statistical Analysis of the Spatial Distribution of Hotspots

To test whether the likelihood that two hotspots arising from the same axon were of similar distance from the soma, compared with the likelihood of this event for randomly chosen hotspots, we plotted the distance from soma of each hotspot versus all other hotspots (n = 3199 pairwise comparisons of the longer versus smaller distance). This analysis was then repeated for the subset of hotspots that arose from the same axon (n = 15 pairwise comparisons). To evaluate the likelihood that the correlation of the same-axon distribution (r^2 = 0.33) was significantly larger than that of the all-hotspot distribution (r^2 = 0.19), we employed a bootstrap analysis. The all-hotspot data set was randomly resampled into 1000 data sets each consisting of 15 pairwise comparisons. The resulting R^2 values of all fits ranged from 0.0 to 0.84, with 32% of the values $\geq$0.33. Thus we concluded that the difference in correlation was insignificant.

For analysis of hotspot distance relative to dendritic branch points, we compared the median distance from the nearest branch point of all hotspots (n = 81, resampled 100 times) to the median distance from branch point of the dendritic arbor density, using only hotspot-bearing dendrites. To ensure that the disproportionate expression of hotspots close to branch points was not an artifact of their distribution close to the soma, where more branch points typically occur, the dendritic density function was truncated at 150 μm from the nearest branch point, the furthest distance at which any hotspots were found. Using the entire dendritic arbor produced an even greater disparity between hotspot and dendrite density distributions (data not shown).

Electron Microscopy

One adult animal expressing both Cre under control of the parvalbumin (PV) promoter (Hippenmeyer et al., 2005) and the reporter Rosa-tdTomato (Jackson Labs 007914) (Madisen et al., 2010) to label PV+ neurons was used for electron microscopy. The animal was perfused with heparin (10 U/mL) in PBS followed by 4% paraformaldehyde and 0.5% glutaraldehyde in PBS. The brain was removed and postfixed overnight in 4% paraformaldehyde before being sectioned at 60 um in ice-cold PBS on a Leica VT1000 vibratome using the same cutting angles as for physiology. Sections were treated with glycine (100 mM) in PBS for 15 min. Antigen retrieval was carried out by microwaving sections at 50°C for 5 min, resting them for 5 min, and repeating, in 10 mM Na-citrate buffer (pH 6.0). Blocking buffer (1.5% normal goat serum, 1% bovine serum albumin in PBS) was applied for 30 min. To immunostain PV-tdTomato neurons and thalamic afferents, the following reagents (Vector Labs except as noted) were applied in sequence with PBS washes between steps: Rabbit anti-RFP (1:1000, 14 hr, 4°C; Abcam); biotinylated goat anti-rabbit (0.5%, 2 hr); avidin-biotin reaction (2 hr; Vector ABC kit); the chromogen VIP (10 min) (Zhou and Grofova, 1995); 0.5% Na azide; guinea pig anti-VGluT2 (1:2000, 14 hr, 4°C; Chemicon); biotinylated goat anti-guinea pig secondary (0.5%, 2 hr); DAB (10 min).

Slices were fixed in 1% OsO_4 on ice for 1 hr. Slices were washed in cold ddH_2O and passed through a series of cold ethanol solutions of (70%, 90%, 100% (2×); 10 min each). The slices were then treated with cold dry acetone for 10 min and room temperature acetone for 10 min, followed by 50:50 acetone:Durcupan ACM resin overnight and then 100% Durcupan overnight. The slices were flat-embedded between glass slides treated with liquid release agent (Ted Pella) and left in oven at 60°C for 2 days.

A block of layer 4 in barrel cortex was trimmed and ribbons of serial thin sections (80 nm) were cut on a Leica Ultracut UCT using a diamond knife (Diatome). Ribbons were collected on formvar-coated slot grids and poststained with 1% aqueous uranyl acetate and Sato lead. TEM images were collected on a 1200EX JEOL microscope at 20,000× magnification. Negatives were digitized with a Flextight scanner at 1500 dpi, contrast and brightness were adjusted in Adobe Photoshop, and volume reconstruction was performed using Reconstruct (Fiala, 2005).

Modeling

Three neurons were selected based on physiology and completeness of fill for further reconstruction, including process thickness, of the dendritic arbor and the initial ~1/3 of the axon. Tracings were imported into NEURON 7 (Hines and Carnevale, 1997) using the Import3D tool and endowed with specific membrane capacitance of 1 $\mu F/cm^2$, intracellular resistivity of 170 Ω-cm, and passive leak conductance of 130 $\mu S/cm^2$ (soma and dendrites) or 6 $\mu S/cm^2$ (axon) (Nörenberg et al., 2010). The d-λ method was used to set segment partitioning such that the length of each segment was <1% of the alternating current length constant at 1 kHz (Carnevale and Hines, 2006).

Synaptic conductances were simulated using a custom dynamic clamp (A. Gartland). Sixteen conductances with reversal potential of 0 mV were attached across the dendritic arbor so that the statistics of their distribution approximately matched the statistics of hotspots from reconstructed neurons (model: median distance from soma, 49 μm, 5th to 95th percentile 17–02 μm; data: median 50 μm, 5th to 95th percentile 15–115 μm). For the single electrode configuration, each of the 16 loci was tested in turn; for the 2, 4, and 8 electrode configurations, 8–16 possible configurations were tested.

SUPPLEMENTAL INFORMATION

Supplemental Information includes five figures and Supplemental Experimental Procedures and can be found with this article online at doi:10.1016/j.neuron.2011.05.032.

ACKNOWLEDGMENTS

We are grateful to J. Isaacson, the members of the Scanziani and Isaacson laboratories, and D. DiGregorio for discussion of this work, to P. Abelkop for histological help, to R. Malinow and H. Makino for use of the two-photon microscope, and to J. Evora for mouse colony support. A. Gartland contributed code for simulation of conductance injection in the NEURON modeling environment. This work was supported by a training grant to M.W.B. (NS007220), a postdoctoral National Research Service Award fellowship to C.H. (NS060585), National Center for Research Resources grant 5P41RR004050 to M.H.E., NIH grant MH070058 to M.S., the Gatsby Charitable Foundation, and the Howard Hughes Medical Institute.

Accepted: May 9, 2011
Published: July 13, 2011

REFERENCES

Agmon, A., and Connors, B.W. (1991). Thalamocortical responses of mouse somatosensory (barrel) cortex in vitro. Neuroscience *41*, 365–379.

Ahmed, B., Anderson, J.C., Martin, K.A., and Nelson, J.C. (1997). Map of the synapses onto layer 4 basket cells of the primary visual cortex of the cat. J. Comp. Neurol. *380*, 230–242.

Beierlein, M., Gibson, J.R., and Connors, B.W. (2003). Two dynamically distinct inhibitory networks in layer 4 of the neocortex. J. Neurophysiol. *90*, 2987–3000.

Benshalom, G., and White, E.L. (1986). Quantification of thalamocortical synapses with spiny stellate neurons in layer IV of mouse somatosensory cortex. J. Comp. Neurol. *253*, 303–314.

Bollmann, J.H., and Engert, F. (2009). Subcellular topography of visually driven dendritic activity in the vertebrate visual system. Neuron *61*, 895–905.

Bruno, R.M., and Simons, D.J. (2002). Feedforward mechanisms of excitatory and inhibitory cortical receptive fields. J. Neurosci. *22*, 10966–10975.

Carnevale, N.T., and Hines, M.L. (2006). The Neuron Book (Cambridge: Cambridge University Press).

Chalifoux, J.R., and Carter, A.G. (2010). GABAB receptors modulate NMDA receptor calcium signals in dendritic spines. Neuron *66*, 101–113.

Cruikshank, S.J., Lewis, T.J., and Connors, B.W. (2007). Synaptic basis for intense thalamocortical activation of feedforward inhibitory cells in neocortex. Nat. Neurosci. *10*, 462–468.

DiGregorio, D.A., Nusser, Z., and Silver, R.A. (2002). Spillover of glutamate onto synaptic AMPA receptors enhances fast transmission at a cerebellar synapse. Neuron *35*, 521–533.

Euler, T., Detwiler, P.B., and Denk, W. (2002). Directionally selective calcium signals in dendrites of starburst amacrine cells. Nature *418*, 845–852.

Fiala, J.C. (2005). Reconstruct: a free editor for serial section microscopy. J. Microsc. *218*, 52–61.

Fontanez, D.E., and Porter, J.T. (2006). Adenosine A1 receptors decrease thalamic excitation of inhibitory and excitatory neurons in the barrel cortex. Neuroscience *137*, 1177–1184.

Foster, K.A., and Regehr, W.G. (2004). Variance-mean analysis in the presence of a rapid antagonist indicates vesicle depletion underlies depression at the climbing fiber synapse. Neuron *43*, 119–131.

Fremeau, R.T., Jr., Troyer, M.D., Pahner, I., Nygaard, G.O., Tran, C.H., Reimer, R.J., Bellocchio, E.E., Fortin, D., Storm-Mathisen, J., and Edwards, R.H. (2001). The expression of vesicular glutamate transporters defines two classes of excitatory synapse. Neuron *31*, 247–260.

Fried, S.I., Münch, T.A., and Werblin, F.S. (2002). Mechanisms and circuitry underlying directional selectivity in the retina. Nature *420*, 411–414.

Gabernet, L., Jadhav, S.P., Feldman, D.E., Carandini, M., and Scanziani, M. (2005). Somatosensory integration controlled by dynamic thalamocortical feed-forward inhibition. Neuron *48*, 315–327.

Geiger, J.R., Lübke, J., Roth, A., Frotscher, M., and Jonas, P. (1997). Submillisecond AMPA receptor-mediated signaling at a principal neuron-interneuron synapse. Neuron *18*, 1009–1023.

Gibson, J.R., Beierlein, M., and Connors, B.W. (1999). Two networks of electrically coupled inhibitory neurons in neocortex. Nature *402*, 75–79.

Gil, Z., Connors, B.W., and Amitai, Y. (1999). Efficacy of thalamocortical and intracortical synaptic connections: quanta, innervation, and reliability. Neuron *23*, 385–397.

Goldberg, J.H., Tamas, G., Aronov, D., and Yuste, R. (2003a). Calcium microdomains in aspiny dendrites. Neuron *40*, 807–821.

Goldberg, J.H., Tamas, G., and Yuste, R. (2003b). Ca^{2+} imaging of mouse neocortical interneurone dendrites: Ia-type K^{+} channels control action potential backpropagation. J. Physiol. *551*, 49–65.

Gouwens, N.W., and Wilson, R.I. (2009). Signal propagation in Drosophila central neurons. J. Neurosci. *29*, 6239–6249.

Gulyás, A.I., Miles, R., Sík, A., Tóth, K., Tamamaki, N., and Freund, T.F. (1993). Hippocampal pyramidal cells excite inhibitory neurons through a single release site. Nature *366*, 683–687.

Higley, M.J., Soler-Llavina, G.J., and Sabatini, B.L. (2009). Cholinergic modulation of multivesicular release regulates striatal synaptic potency and integration. Nat. Neurosci. *12*, 1121–1128.

Hines, M.L., and Carnevale, N.T. (1997). The NEURON simulation environment. Neural Comput. *9*, 1179–1209.

Hippenmeyer, S., Vrieseling, E., Sigrist, M., Portmann, T., Laengle, C., Ladle, D.R., and Arber, S. (2005). A developmental switch in the response of DRG neurons to ETS transcription factor signaling. PLoS Biol. *3*, e159.

Hu, H., Martina, M., and Jonas, P. (2010). Dendritic mechanisms underlying rapid synaptic activation of fast-spiking hippocampal interneurons. Science *327*, 52–58.

Hull, C., Isaacson, J.S., and Scanziani, M. (2009). Postsynaptic mechanisms govern the differential excitation of cortical neurons by thalamic inputs. J. Neurosci. *29*, 9127–9136.

Hur, E.E., and Zaborszky, L. (2005). Vglut2 afferents to the medial prefrontal and primary somatosensory cortices: a combined retrograde tracing in situ hybridization study [corrected]. J. Comp. Neurol. *483*, 351–373.

Inoue, T., and Imoto, K. (2006). Feedforward inhibitory connections from multiple thalamic cells to multiple regular-spiking cells in layer 4 of the somatosensory cortex. J. Neurophysiol. *96*, 1746–1754.

Jia, H., Rochefort, N.L., Chen, X., and Konnerth, A. (2010). Dendritic organization of sensory input to cortical neurons in vivo. Nature *464*, 1307–1312.

Kharazia, V.N., and Weinberg, R.J. (1994). Glutamate in thalamic fibers terminating in layer IV of primary sensory cortex. J. Neurosci. *14*, 6021–6032.

Koester, H.J., and Johnston, D. (2005). Target cell-dependent normalization of transmitter release at neocortical synapses. Science *308*, 863–866.

Kubota, Y., Hatada, S., Kondo, S., Karube, F., and Kawaguchi, Y. (2007). Neocortical inhibitory terminals innervate dendritic spines targeted by thalamocortical afferents. J. Neurosci. *27*, 1139–1150.

Larkum, M.E., and Nevian, T. (2008). Synaptic clustering by dendritic signalling mechanisms. Curr. Opin. Neurobiol. *18*, 321–331.

Losonczy, A., Makara, J.K., and Magee, J.C. (2008). Compartmentalized dendritic plasticity and input feature storage in neurons. Nature *452*, 436–441.

Madisen, L., Zwingman, T.A., Sunkin, S.M., Oh, S.W., Zariwala, H.A., Gu, H., Ng, L.L., Palmiter, R.D., Hawrylycz, M.J., Jones, A.R., et al. (2010). A robust and high-throughput Cre reporting and characterization system for the whole mouse brain. Nat. Neurosci. *13*, 133–140.

Magee, J.C. (2000). Dendritic integration of excitatory synaptic input. Nat. Rev. Neurosci. *1*, 181–190.

McBride, T.J., Rodriguez-Contreras, A., Trinh, A., Bailey, R., and Debello, W.M. (2008). Learning drives differential clustering of axodendritic contacts in the barn owl auditory system. J. Neurosci. *28*, 6960–6973.

Miles, R., and Poncer, J.C. (1996). Paired recordings from neurones. Curr. Opin. Neurobiol. *6*, 387–394.

Nahmani, M., and Erisir, A. (2005). VGluT2 immunochemistry identifies thalamocortical terminals in layer 4 of adult and developing visual cortex. J. Comp. Neurol. *484*, 458–473.

Nörenberg, A., Hu, H., Vida, I., Bartos, M., and Jonas, P. (2010). Distinct nonuniform cable properties optimize rapid and efficient activation of fast-spiking GABAergic interneurons. Proc. Natl. Acad. Sci. USA *107*, 894–899.

Peron, S.P., Jones, P.W., and Gabbiani, F. (2009). Precise subcellular input retinotopy and its computational consequences in an identified visual interneuron. Neuron *63*, 830–842.

Petersen, R.S., Brambilla, M., Bale, M.R., Alenda, A., Panzeri, S., Montemurro, M.A., and Maravall, M. (2008). Diverse and temporally precise kinetic feature selectivity in the VPm thalamic nucleus. Neuron *60*, 890–903.

Pinto, D.J., Hartings, J.A., Brumberg, J.C., and Simons, D.J. (2003). Cortical damping: analysis of thalamocortical response transformations in rodent barrel cortex. Cereb. Cortex *13*, 33–44.

Poirazi, P., and Mel, B.W. (2001). Impact of active dendrites and structural plasticity on the memory capacity of neural tissue. Neuron *29*, 779–796.

Polsky, A., Mel, B.W., and Schiller, J. (2004). Computational subunits in thin dendrites of pyramidal cells. Nat. Neurosci. *7*, 621–627.

Porter, J.T., Johnson, C.K., and Agmon, A. (2001). Diverse types of interneurons generate thalamus-evoked feedforward inhibition in the mouse barrel cortex. J. Neurosci. *21*, 2699–2710.

Pouille, F., and Scanziani, M. (2001). Enforcement of temporal fidelity in pyramidal cells by somatic feed-forward inhibition. Science *293*, 1159–1163.

Pouille, F., Marin-Burgin, A., Adesnik, H., Atallah, B.V., and Scanziani, M. (2009). Input normalization by global feedforward inhibition expands cortical dynamic range. Nat. Neurosci. *12*, 1577–1585.

Rall, W. (1970). Cable properties of dendrites and effects of synaptic location. In Excitatory Synaptic Mechanisms, P. Anderson and J.K.S. Jansen, eds. (Oslo, Norway: Universitetsforlaget), pp. 175–186.

Richardson, R.J., Blundon, J.A., Bayazitov, I.T., and Zakharenko, S.S. (2009). Connectivity patterns revealed by mapping of active inputs on dendrites of thalamorecipient neurons in the auditory cortex. J. Neurosci. *29*, 6406–6417.

Salin, P.A., Scanziani, M., Malenka, R.C., and Nicoll, R.A. (1996). Distinct short-term plasticity at two excitatory synapses in the hippocampus. Proc. Natl. Acad. Sci. USA *93*, 13304–13309.

Saviane, C., and Silver, R.A. (2006). Fast vesicle reloading and a large pool sustain high bandwidth transmission at a central synapse. Nature *439*, 983–987.

Segev, I., and London, M. (2000). Untangling dendrites with quantitative models. Science *290*, 744–750.

Silver, R.A. (2003). Estimation of nonuniform quantal parameters with multiple-probability fluctuation analysis: theory, application and limitations. J. Neurosci. Methods *130*, 127–141.

Silver, R.A., Lubke, J., Sakmann, B., and Feldmeyer, D. (2003). High-probability uniquantal transmission at excitatory synapses in barrel cortex. Science *302*, 1981–1984.

Staiger, J.F., Zilles, K., and Freund, T.F. (1996). Distribution of GABAergic elements postsynaptic to ventroposteromedial thalamic projections in layer IV of rat barrel cortex. Eur. J. Neurosci. *8*, 2273–2285.

Stratford, K.J., Tarczy-Hornoch, K., Martin, K.A., Bannister, N.J., and Jack, J.J. (1996). Excitatory synaptic inputs to spiny stellate cells in cat visual cortex. Nature *382*, 258–261.

Sun, Q.Q., Huguenard, J.R., and Prince, D.A. (2006). Barrel cortex microcircuits: thalamocortical feedforward inhibition in spiny stellate cells is mediated by a small number of fast-spiking interneurons. J. Neurosci. *26*, 1219–1230.

Swadlow, H.A., and Gusev, A.G. (2000). The influence of single VB thalamocortical impulses on barrel columns of rabbit somatosensory cortex. J. Neurophysiol. *83*, 2802–2813.

Swadlow, H.A., and Gusev, A.G. (2002). Receptive-field construction in cortical inhibitory interneurons. Nat. Neurosci. *5*, 403–404.

Tamás, G., Szabadics, J., and Somogyi, P. (2002). Cell type- and subcellular position-dependent summation of unitary postsynaptic potentials in neocortical neurons. J. Neurosci. *22*, 740–747.

Tan, Z., Hu, H., Huang, Z.J., and Agmon, A. (2008). Robust but delayed thalamocortical activation of dendritic-targeting inhibitory interneurons. Proc. Natl. Acad. Sci. USA *105*, 2187–2192.

Tong, G., and Jahr, C.E. (1994). Multivesicular release from excitatory synapses of cultured hippocampal neurons. Neuron *12*, 51–59.

Wadiche, J.I., and Jahr, C.E. (2001). Multivesicular release at climbing fiber-Purkinje cell synapses. Neuron *32*, 301–313.

Wehr, M., and Zador, A.M. (2003). Balanced inhibition underlies tuning and sharpens spike timing in auditory cortex. Nature *426*, 442–446.

White, E.L., and Rock, M.P. (1981). A comparison of thalamocortical and other synaptic inputs to dendrites of two non-spiny neurons in a single barrel of mouse SmI cortex. J. Comp. Neurol. *195*, 265–277.

White, E.L., Benshalom, G., and Hersch, S.M. (1984). Thalamocortical and other synapses involving nonspiny multipolar cells of mouse SmI cortex. J. Comp. Neurol. *229*, 311–320.

Wilent, W.B., and Contreras, D. (2005). Dynamics of excitation and inhibition underlying stimulus selectivity in rat somatosensory cortex. Nat. Neurosci. *8*, 1364–1370.

Williams, S.R., and Stuart, G.J. (2003). Role of dendritic synapse location in the control of action potential output. Trends Neurosci. *26*, 147–154.

Zhou, M., and Grofova, I. (1995). The use of peroxidase substrate Vector VIP in electron microscopic single and double antigen localization. J. Neurosci. Methods *62*, 149–158.